



Study of η – η' mixing from measurement of $B_{(s)}^0 \rightarrow J/\psi \eta^{(\prime)}$ decay rates

The LHCb collaboration[†]

Abstract

A study of B^0 and B_s^0 meson decays into $J/\psi\eta$ and $J/\psi\eta'$ final states is performed using a data set of proton-proton collisions at centre-of-mass energies of 7 and 8 TeV, collected by the LHCb experiment and corresponding to 3.0 fb^{-1} of integrated luminosity. The decay $B^0 \rightarrow J/\psi\eta'$ is observed for the first time. The following ratios of branching fractions are measured:

$$\frac{\mathcal{B}(B^0 \rightarrow J/\psi\eta')}{\mathcal{B}(B_s^0 \rightarrow J/\psi\eta')} = (2.28 \pm 0.65 \text{ (stat)} \pm 0.10 \text{ (syst)} \pm 0.13 (f_s/f_d)) \times 10^{-2},$$

$$\frac{\mathcal{B}(B^0 \rightarrow J/\psi\eta)}{\mathcal{B}(B_s^0 \rightarrow J/\psi\eta)} = (1.85 \pm 0.61 \text{ (stat)} \pm 0.09 \text{ (syst)} \pm 0.11 (f_s/f_d)) \times 10^{-2},$$

where the third uncertainty is related to the present knowledge of f_s/f_d , the ratio between the probabilities for a b quark to form a B_s^0 or a B^0 meson. The branching fraction ratios are used to determine the parameters of $\eta - \eta'$ meson mixing. In addition, the first evidence for the decay $B_s^0 \rightarrow \psi(2S)\eta'$ is reported, and the relative branching fraction is measured,

$$\frac{\mathcal{B}(B_s^0 \rightarrow \psi(2S)\eta')}{\mathcal{B}(B_s^0 \rightarrow J/\psi\eta')} = (38.7 \pm 9.0 \text{ (stat)} \pm 1.3 \text{ (syst)} \pm 0.9(\mathcal{B})) \times 10^{-2},$$

where the third uncertainty is due to the limited knowledge of the branching fractions of J/ψ and $\psi(2S)$ mesons.

Submitted to JHEP

© CERN on behalf of the LHCb collaboration, license CC-BY-4.0.

[†]Authors are listed at the end of this paper.

1 Introduction

Decays of beauty mesons to two-body final states containing a charmonium resonance (J/ψ , $\psi(2S)$, χ_c , η_c , ...) allow the study of electroweak transitions, of which those sensitive to charge-parity violation are especially interesting. In addition, a study of these decays provides insight into strong interactions at low-energy scales. The hypothesis that η and η' mesons contain gluonic and intrinsic $c\bar{c}$ components has long been used to explain experimental results, including the recent observations of large branching fractions for some decay processes of J/ψ and B mesons into pseudoscalar mesons [1, 2].

The rates of $B_{(s)}^0 \rightarrow J/\psi \eta^{(\prime)}$ decays are of particular importance because of their relation to the $\eta - \eta'$ mixing parameters and to a possible contribution of gluonic components in the η' meson [1, 3, 4]. These decays proceed via formation of a $\eta^{(\prime)}$ state from $d\bar{d}$ (for B^0 mesons) and $s\bar{s}$ (for B_s^0 mesons) quark pairs (see Fig. 1).

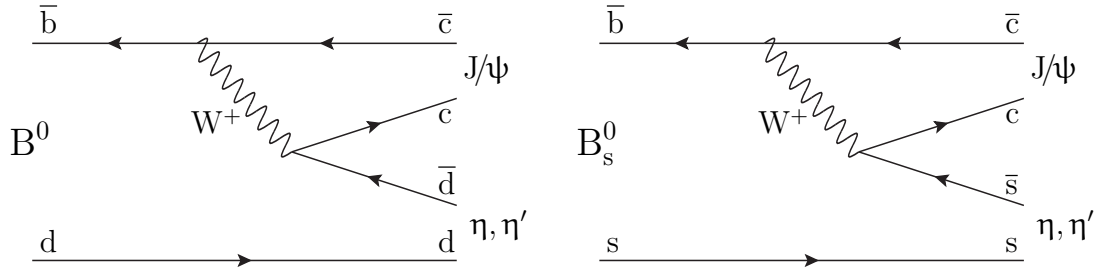


Figure 1: Leading-order Feynman diagrams for the decays $B_{(s)}^0 \rightarrow J/\psi \eta^{(\prime)}$.

The physical $\eta^{(\prime)}$ states are described in terms of isospin singlet states $|\eta_q\rangle = \frac{1}{\sqrt{2}} (|u\bar{u}\rangle + |d\bar{d}\rangle)$ and $|\eta_s\rangle = |s\bar{s}\rangle$, the glueball state $|gg\rangle$, and two mixing angles φ_P and φ_G [5–7],

$$|\eta\rangle = \cos \varphi_P |\eta_q\rangle - \sin \varphi_P |\eta_s\rangle, \quad (1a)$$

$$|\eta'\rangle = \cos \varphi_G (\sin \varphi_P |\eta_q\rangle + \cos \varphi_P |\eta_s\rangle) + \sin \varphi_G |gg\rangle. \quad (1b)$$

The contribution of the $|gg\rangle$ state to the physical η state is expected to be highly suppressed [8–12], and is therefore omitted from Eq. (1a). The mixing angles can be related to the $B_{(s)}^0 \rightarrow J/\psi \eta^{(\prime)}$ decay rates [3],

$$\tan^4 \varphi_P = \frac{R'}{R'_s}, \quad \cos^4 \varphi_G = R' R'_s, \quad (2)$$

where

$$R'_{(s)} \equiv R_{(s)} \left(\frac{\Phi_{(s)}^\eta}{\Phi_{(s)}^{\eta'}} \right)^3, \quad R_{(s)} \equiv \frac{\mathcal{B}(B_{(s)}^0 \rightarrow J/\psi \eta')}{\mathcal{B}(B_{(s)}^0 \rightarrow J/\psi \eta)}, \quad (3)$$

and $\Phi_{(s)}^{\eta^{(\prime)}}$ are phase-space factors for the $B_{(s)}^0 \rightarrow J/\psi \eta^{(\prime)}$ decays.

Table 1: Mixing angles φ_G and φ_P (in degrees). The third column corresponds to measurements where the gluonic component is neglected. Total uncertainties are quoted.

Refs.	φ_P	φ_G	$\varphi_P(\varphi_G = 0)$
[6, 7, 17–23]	–	–	37.7–41.5
[24, 26]	41.4 ± 1.3	12 ± 13	41.5 ± 1.2
[27]	44.6 ± 4.4	$32 \begin{smallmatrix} + \\ - \end{smallmatrix} \begin{smallmatrix} 11 \\ 22 \end{smallmatrix}$	40.7 ± 2.3
[1, 28, 29]	40.0 ± 3.0	23.3 ± 31.6	37.7 ± 2.6
[14]	–	–	$< 42.2 @ 90\% \text{ CL}$
[16]	–	–	$45.5 \begin{smallmatrix} + \\ - \end{smallmatrix} \begin{smallmatrix} 1.8 \\ 1.5 \end{smallmatrix}$

The results for the mixing angles obtained from analyses of $B_{(s)}^0 \rightarrow J/\psi \eta^{(\prime)}$ decays [13–16] are summarised in Table 1, together with references to the corresponding measurements based on J/ψ and light meson decays [6, 7, 17–27] and semileptonic D meson decays [1, 28, 29]. The important role of $\eta - \eta'$ mixing in decays of charm mesons to a pair of light pseudoscalar mesons as well as decays into a light pseudoscalar and vector meson is discussed in Refs. [30–32]. The $\eta - \eta'$ mixing was previously studied in colour-suppressed B decays to open charm [33] and experiments on π^- and K^- beams [34].

In this paper, the measurement of the ratios of branching fractions for $B_{(s)}^0 \rightarrow \psi \eta^{(\prime)}$ decays is presented, where ψ represents either the J/ψ or $\psi(2S)$ meson, and charge-conjugate decays are implicitly included. The study uses a sample corresponding to 3.0 fb^{-1} of pp collision data, collected with the LHCb detector [35] at centre-of-mass energies of 7 TeV in 2011 and 8 TeV in 2012. The results are reported as

$$\begin{aligned}
 R_{\eta'} &\equiv \frac{\mathcal{B}(B^0 \rightarrow J/\psi \eta')}{\mathcal{B}(B_s^0 \rightarrow J/\psi \eta')}, & R_{\eta} &\equiv \frac{\mathcal{B}(B^0 \rightarrow J/\psi \eta)}{\mathcal{B}(B_s^0 \rightarrow J/\psi \eta)}, \\
 R &\equiv \frac{\mathcal{B}(B^0 \rightarrow J/\psi \eta')}{\mathcal{B}(B^0 \rightarrow J/\psi \eta)}, & R_s &\equiv \frac{\mathcal{B}(B_s^0 \rightarrow J/\psi \eta')}{\mathcal{B}(B_s^0 \rightarrow J/\psi \eta)}, \\
 R_{\psi(2S)} &\equiv \frac{\mathcal{B}(B_s^0 \rightarrow \psi(2S) \eta')}{\mathcal{B}(B_s^0 \rightarrow J/\psi \eta')}.
 \end{aligned} \tag{4}$$

Due to the similar kinematic properties, decay topology and selection requirements applied, many systematic uncertainties cancel in the ratios.

2 LHCb detector and simulation

The LHCb detector [35] is a single-arm forward spectrometer covering the pseudorapidity range $2 < \eta < 5$, designed for the study of particles containing b or c quarks. The detector includes a high-precision tracking system consisting of a silicon-strip vertex detector surrounding the pp interaction region [36], a large-area silicon-strip detector located upstream of a dipole magnet with a bending power of about 4 Tm, and three stations of silicon-strip detectors and straw drift tubes [37] placed downstream of the magnet.

The tracking system provides a measurement of momentum, p , with a relative uncertainty that varies from 0.4% at low momentum to 0.6% at 100 GeV/ c . The minimum distance of a track to a primary vertex (PV), the impact parameter, is measured with a resolution of $(15 + 29/p_T) \mu\text{m}$, where p_T is the component of momentum transverse to the beam, in GeV/ c . Different types of charged hadrons are distinguished using information from two ring-imaging Cherenkov detectors [38]. Photon, electron and hadron candidates are identified by a calorimeter system consisting of a scintillating-pad detector (SPD), preshower detectors (PS), an electromagnetic calorimeter and a hadronic calorimeter. Muons are identified by a system composed of alternating layers of iron and multiwire proportional chambers [39].

This analysis uses events collected by triggers that select the $\mu^+\mu^-$ pair from the ψ decay with high efficiency. At the hardware stage a muon with $p_T > 1.5$ GeV/ c or a pair of muons is required to trigger the event. For dimuon candidates, the product of the p_T of muon candidates is required to satisfy $\sqrt{p_{T1}p_{T2}} > 1.3$ GeV/ c and $\sqrt{p_{T1}p_{T2}} > 1.6$ GeV/ c for data collected at $\sqrt{s} = 7$ and 8 TeV, respectively. At the subsequent software trigger stage, two muons are selected with a mass in excess of 2.97 GeV/ c^2 and consistent with originating from a common vertex. The common vertex is required to be significantly displaced from the pp collision vertices.

In the simulation, pp collisions are generated using PYTHIA [40] with a specific LHCb configuration [41]. Decays of hadronic particles are described by EVTGEN [42], in which final-state radiation is generated using PHOTOS [43]. The interaction of the generated particles with the detector, and its response, are implemented using the GEANT4 toolkit [44] as described in Ref. [45].

3 Event selection

Signal decays are reconstructed using the $\psi \rightarrow \mu^+\mu^-$ decay. For the $B_{(s)}^0 \rightarrow \psi\eta'$ channels, η' candidates are reconstructed using the $\eta' \rightarrow \rho^0\gamma$ and $\eta' \rightarrow \eta\pi^+\pi^-$ decays, followed by $\rho^0 \rightarrow \pi^+\pi^-$ and $\eta \rightarrow \gamma\gamma$ decays. For the $B_{(s)}^0 \rightarrow J/\psi\eta$ channels, η candidates are reconstructed using the $\eta \rightarrow \pi^+\pi^-\pi^0$ decay, followed by the $\pi^0 \rightarrow \gamma\gamma$ decays. The $\eta \rightarrow \gamma\gamma$ decay, which has a larger branching fraction and reconstruction efficiency, is not used for the reconstruction of $B_{(s)}^0 \rightarrow J/\psi\eta$ candidates due to a worse mass resolution, which does not allow to resolve the B_s^0 and B^0 peaks [16, 46]. The selection criteria, which follow Refs. [16, 46], are common to all decay channels, except for the requirements directly related to the photon kinematic properties.

The muons and pions must be positively identified using the combined information from RICH, calorimeter, and muon detectors [47, 48]. Pairs of oppositely charged particles, identified as muons, each having $p_T > 550$ MeV/ c and originating from a common vertex, are combined to form $\psi \rightarrow \mu^+\mu^-$ candidates. The resulting dimuon candidate is required to form a good-quality vertex and to have mass between -5σ and $+3\sigma$ around the known J/ψ or $\psi(2S)$ masses, where the mass resolution σ is around 13 MeV/ c^2 . The asymmetric mass intervals include the low-mass tail due to final-state radiation.

The charged pions are required to have $p_T > 250 \text{ MeV}/c$ and to be inconsistent with being produced in any primary vertex. Photons are selected from neutral energy clusters in the electromagnetic calorimeter, *i.e.* clusters that do not match the geometrical extrapolation of any track [48]. The photon quality criteria are further refined by exploiting information from the PS and SPD detectors. The photon candidate’s transverse momentum inferred from the energy deposit is required to be greater than $500 \text{ MeV}/c$ for $\eta' \rightarrow \rho^0\gamma$ and $\eta \rightarrow \gamma\gamma$ candidates, and $250 \text{ MeV}/c$ for $\pi^0 \rightarrow \gamma\gamma$ candidates. In order to suppress the large combinatorial background from $\pi^0 \rightarrow \gamma\gamma$ decays, photons that, when combined with another photon in the event, form a $\pi^0 \rightarrow \gamma\gamma$ candidate with mass within $25 \text{ MeV}/c^2$ of the π^0 mass (corresponding to about $\pm 3\sigma$ around the known mass) are not used in the reconstruction of $\eta' \rightarrow \rho^0\gamma$ candidates. The $\pi^+\pi^-$ mass for the $\eta' \rightarrow \rho^0\gamma$ channel is required to be between 570 and $920 \text{ MeV}/c^2$. Finally, the masses of π^0 , η and η' candidates are required to be within $\pm 25 \text{ MeV}/c^2$, $\pm 70 \text{ MeV}/c^2$ and $\pm 60 \text{ MeV}/c^2$ from the known values [49], where each range corresponds approximately to a $\pm 3\sigma$ interval.

The $B_{(s)}^0$ candidates are formed from $\psi\eta^{(\prime)}$ combinations with $p_T(\eta^{(\prime)}) > 2.5 \text{ GeV}/c$. To improve the mass resolution, a kinematic fit is applied [50]. This fit constrains the masses of intermediate narrow resonances to their known values [49], and requires the $B_{(s)}^0$ candidate’s momentum to point back to the PV. A requirement on the quality of this fit is applied in order to further suppress background.

Finally, the measured proper decay time of the $B_{(s)}^0$ candidate, calculated with respect to the associated primary vertex, is required to be between $0.1 \text{ mm}/c$ and $2.0 \text{ mm}/c$. The upper limit is used to remove poorly reconstructed candidates.

4 Study of $B_{(s)}^0 \rightarrow J/\psi \eta'$ and $B_{(s)}^0 \rightarrow J/\psi \eta$ decays with $\eta' \rightarrow \eta\pi^+\pi^-$ and $\eta \rightarrow \pi^+\pi^-\pi^0$

The mass distributions of the selected $B_{(s)}^0 \rightarrow J/\psi \eta'$ and $B_{(s)}^0 \rightarrow J/\psi \eta$ candidates are shown in Fig. 2, where the η' and η states are reconstructed in the $\eta\pi^+\pi^-$ and $\pi^0\pi^+\pi^-$ decay modes, respectively. The $B_{(s)}^0 \rightarrow J/\psi \eta^{(\prime)}$ signal yields are estimated by unbinned extended maximum-likelihood fits. The B_s^0 and B^0 signals are modelled by a modified Gaussian function with power-law tails on both sides [51], referred to as “ \mathcal{F} function” throughout the paper. The mass resolutions of the B_s^0 and B^0 peaks are the same; the difference of the peak positions is fixed to the known difference between the B_s^0 and the B^0 meson masses [49] and the tail parameters are fixed to simulation predictions. The background contribution is modelled by an exponential function. The fit results are presented in Table 2. For both final states, the fitted position of the B_s^0 peak is consistent with the known B_s^0 mass [49] and the mass resolution is consistent with simulations.

The significance for the low-yield B^0 decays is determined by simulating a large number of simplified experiments containing only background. The probability for the background fluctuating to yield a narrow excess consisting of at least the number of observed events is 2.6×10^{-6} (2.0×10^{-4}), corresponding to a significance of 4.7 (3.7) standard deviations in

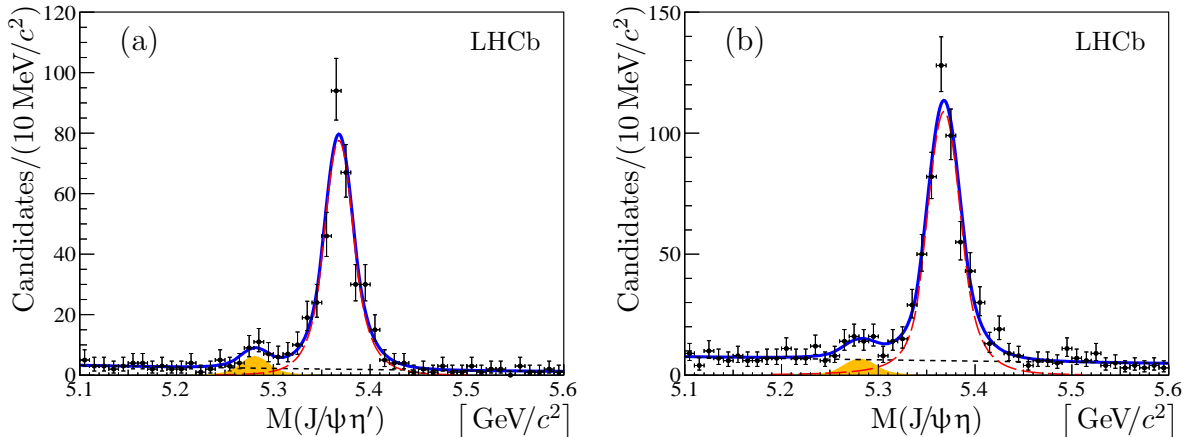


Figure 2: Mass distributions of (a) $B_{(s)}^0 \rightarrow J/\psi \eta'$ and (b) $B_{(s)}^0 \rightarrow J/\psi \eta$ candidates. The decays $\eta' \rightarrow \eta \pi^+ \pi^-$ and $\eta \rightarrow \pi^+ \pi^- \pi^0$ are used in the reconstruction of $J/\psi \eta'$ and $J/\psi \eta$ candidates, respectively. The total fit function (solid blue) and the combinatorial background contribution (dashed black) are shown. The long-dashed red line represents the signal B_s^0 contribution and the yellow shaded area shows the B^0 contribution.

Table 2: Fit results for the numbers of signal events ($N_{B_{(s)}^0}$), B_s^0 signal peak position (m_0) and mass resolution (σ) in $B_{(s)}^0 \rightarrow J/\psi \eta'$ and $B_{(s)}^0 \rightarrow J/\psi \eta$ decays, followed by $\eta' \rightarrow \eta \pi^+ \pi^-$ and $\eta \rightarrow \pi^+ \pi^- \pi^0$ decays, respectively. The quoted uncertainties are statistical only.

Mode	$N_{B_s^0}$	N_{B^0}	m_0 [MeV/ c^2]	σ [MeV/ c^2]
$B_{(s)}^0 \rightarrow J/\psi \eta'$	333 ± 20	26.8 ± 7.5	5367.8 ± 1.1	15.1 ± 1.0
$B_{(s)}^0 \rightarrow J/\psi \eta$	524 ± 27	34 ± 11	5367.9 ± 1.0	17.5 ± 1.1

the $B^0 \rightarrow J/\psi \eta'$ ($B^0 \rightarrow J/\psi \eta$) channel.

To verify that the signal originates from $B_{(s)}^0 \rightarrow J/\psi \eta^{(\prime)}$ decays, the *sPlot* technique is used to disentangle signal and the background components [52]. Using the $\mu^+ \mu^- \pi^+ \pi^- \gamma \gamma$ mass distribution as the discriminating variable, the distributions of the masses of the intermediate resonances are obtained. For each resonance in turn the mass window is released and the mass constraint is removed, keeping other selection criteria as in the baseline analysis. The background-subtracted mass distributions for $\eta' \rightarrow \eta \pi^+ \pi^-$, $\eta \rightarrow \gamma \gamma$ and $J/\psi \rightarrow \mu^+ \mu^-$ combinations from $B_{(s)}^0 \rightarrow J/\psi \eta'$ signal candidates are shown in Fig. 3 and the mass distributions for $\eta \rightarrow \pi^+ \pi^- \pi^0$, $\pi^0 \rightarrow \gamma \gamma$ and $J/\psi \rightarrow \mu^+ \mu^-$ from $B_{(s)}^0 \rightarrow J/\psi \eta$ signal candidates are shown in Fig. 4. Prominent signals are seen for all intermediate resonances. The yields of the various resonances are estimated using unbinned maximum-likelihood fits. The signal shapes are parameterised using \mathcal{F} functions with tail parameters fixed to simulation predictions. The non-resonant component is modelled by a constant function. Due to the small B^0 sample size, the widths of the intermediate

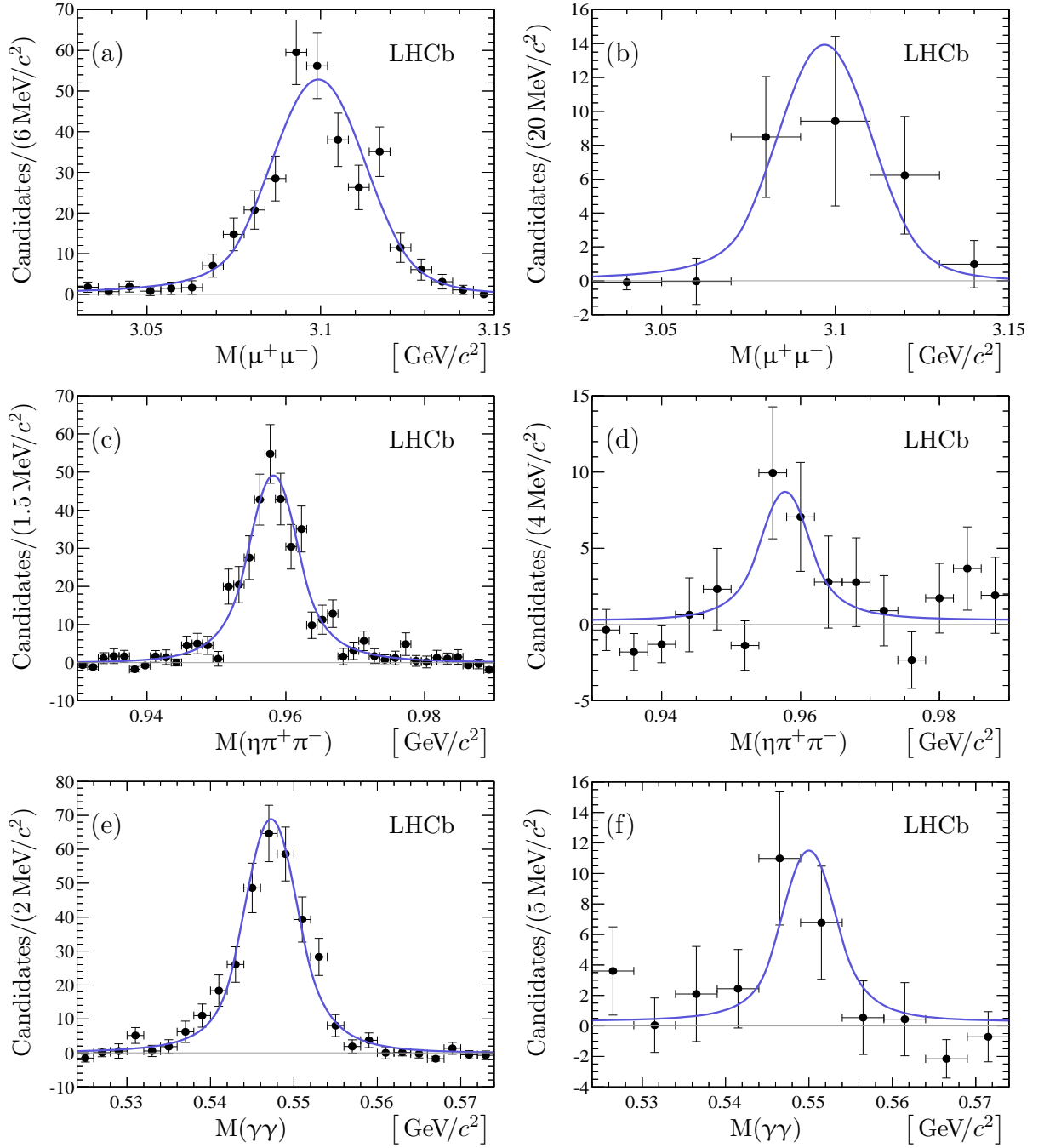


Figure 3: Background subtracted $J/\psi \rightarrow \mu^+ \mu^-$ (a,b), $\eta' \rightarrow \eta \pi^+ \pi^-$ (c,d) and $\eta \rightarrow \gamma \gamma$ (e,f) mass distributions in $B_{(s)}^0 \rightarrow J/\psi \eta'$ decays. The figures (a,c,e) correspond to B_s^0 decays and the figures (b,d,f) correspond to B^0 decays. The solid curves represent the total fit functions.

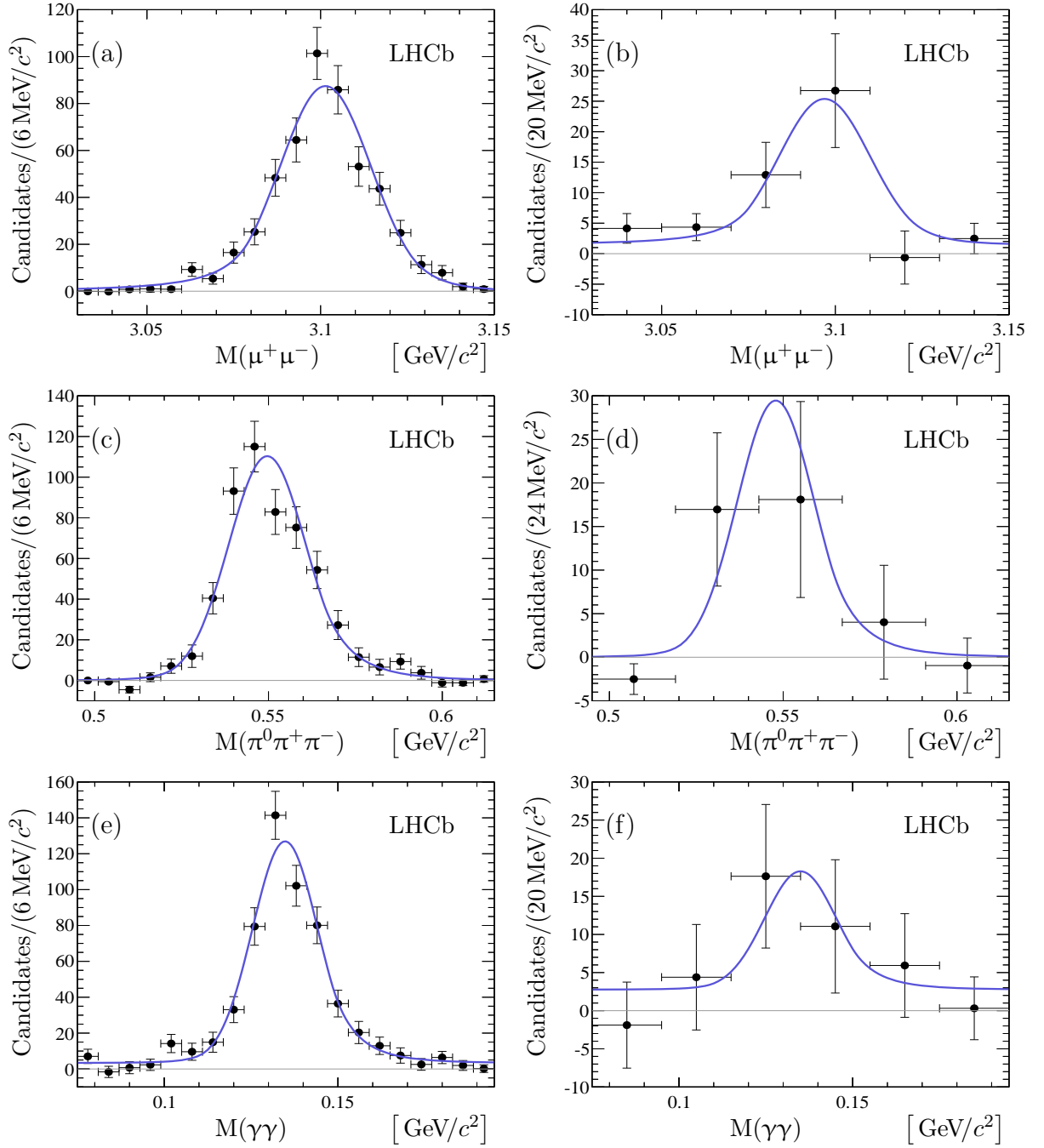


Figure 4: Background subtracted $J/\psi \rightarrow \mu^+\mu^-$ (a,b), $\eta \rightarrow \pi^+\pi^-\pi^0$ (c,d) and $\pi^0 \rightarrow \gamma\gamma$ (e,f) mass distributions in $B_{(s)}^0 \rightarrow J/\psi\eta$ decays. The figures (a,c,d) correspond to B_s^0 decays and the figures (b,d,f) correspond to B^0 decays. The solid curves represent the total fit functions.

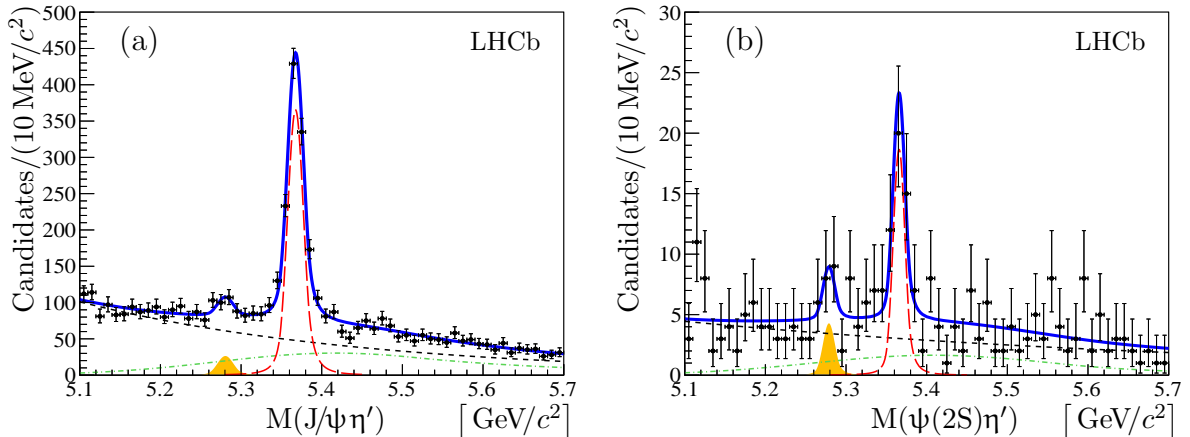


Figure 5: Mass distributions of (a) $B_{(s)}^0 \rightarrow J/\psi \eta'$ and (b) $B_{(s)}^0 \rightarrow \psi(2S) \eta'$ candidates, where the η' state is reconstructed using the $\eta' \rightarrow \rho^0 \gamma$ decay. The total fit function (solid blue) and the combinatorial background contribution (short-dashed black) are shown. The long-dashed red line shows the signal B_s^0 contribution and the yellow shaded area corresponds to the B^0 contribution. The contribution of the reflection from $B^0 \rightarrow \psi K^{*0}$ decays is shown by the green dash-dotted line.

resonances are fixed to the values obtained in the B_s^0 channel, and the peak positions are fixed to the known values [49]. The resulting yields are in agreement with the yields in Table 2, the mass resolutions are consistent with expectations from simulation, and peak positions agree with the known meson masses [49]. The sizes of the non-resonant components are consistent with zero for all cases, supporting the hypothesis of a fully resonant structure for the decays $B_{(s)}^0 \rightarrow J/\psi \eta^{(\prime)}$.

5 Study of $B_{(s)}^0 \rightarrow \psi \eta'$ decays with $\eta' \rightarrow \rho^0 \gamma$

The mass distributions of the selected $\psi \eta'$ candidates, where the η' state is reconstructed using the $\eta' \rightarrow \rho^0 \gamma$ decay, are shown in Fig. 5. The $B_{(s)}^0 \rightarrow \psi \eta'$ signal yields are estimated by unbinned extended maximum-likelihood fits, using the model described in Sect. 4. Studies of the simulation indicate the presence of an additional background due to feed-down from the decay $B^0 \rightarrow \psi K^{*0}$, followed by the $K^{*0} \rightarrow K^+ \pi^-$ decay. The charged kaon is misidentified as a pion and combined with another charged pion and a random photon to form an η' candidate. This background contribution is modelled in the fit using a probability density function obtained from simulation. The fit results are summarised in Table 3. For both final states, the positions of the signal peaks are consistent with the known B_s^0 mass [49] and the mass resolutions agrees with those of the simulation.

The statistical significances of the $B_s^0 \rightarrow \psi(2S) \eta'$ and $B^0 \rightarrow J/\psi \eta'$ signals are determined by a simplified simulation study, as described in Sect. 4. The significances are found to be 4.3σ and 3.5σ for $B_s^0 \rightarrow \psi(2S) \eta'$ and $B^0 \rightarrow J/\psi \eta'$, respectively. By combining the latter

Table 3: Fitted values of the number of signal events ($N_{B_{(s)}^0}$), B_s^0 signal peak position (m_0) and mass resolution (σ) in $B_{(s)}^0 \rightarrow \psi\eta'$ decays, followed by the $\eta' \rightarrow \rho^0\gamma$ decay. The quoted uncertainties are statistical only.

Mode	$N_{B_s^0}$	N_{B^0}	m_0 [MeV/ c^2]	σ [MeV/ c^2]
$B_{(s)}^0 \rightarrow J/\psi\eta'$	988 ± 45	71 ± 22	5367.6 ± 0.5	9.9 ± 0.6
$B_{(s)}^0 \rightarrow \psi(2S)\eta'$	37.4 ± 8.5	8.7 ± 5.1	5365.8 ± 1.9	7.4 ± 1.7

result with the significances of the decay $B^0 \rightarrow J/\psi\eta'$ with $\eta' \rightarrow \eta\pi^+\pi^-$, a total significance of 6.1σ is obtained, corresponding to the first observation of this decay.

The presence of the intermediate resonances is verified following the procedure described in Sect. 4. The resulting mass distributions for $\eta' \rightarrow \rho^0\gamma$ and $\psi \rightarrow \mu^+\mu^-$ candidates from $B_s^0 \rightarrow \psi\eta'$ candidates are shown in Fig. 6, where prominent signals are observed. The signal components are modelled by \mathcal{F} functions. In the $\psi(2S)$ case the means and widths of the signal components are fixed to simulation predictions. The yields of the intermediate resonances are in agreement with the yields from Table 3. The peak positions agree with the known masses [49]. The sizes of the non-resonant components are consistent with zero for all intermediate states, supporting the hypothesis of a fully resonant structure of the decays $B_s^0 \rightarrow \psi\eta'$.

6 Efficiencies and systematic uncertainties

The ratios of branching fractions are measured using the formulae

$$R_{\eta^{(\prime)}} = \frac{N_{B^0 \rightarrow J/\psi\eta^{(\prime)}}}{N_{B_s^0 \rightarrow J/\psi\eta^{(\prime)}}} \frac{\varepsilon_{B_s^0 \rightarrow J/\psi\eta^{(\prime)}}}{\varepsilon_{B^0 \rightarrow J/\psi\eta^{(\prime)}}} \frac{f_s}{f_d}, \quad (5)$$

$$R_{(s)} = \frac{N_{B_{(s)}^0 \rightarrow J/\psi\eta'} \varepsilon_{B_{(s)}^0 \rightarrow J/\psi\eta'} \mathcal{B}(\eta \rightarrow \pi^+\pi^-\pi^0) \mathcal{B}(\pi^0 \rightarrow \gamma\gamma)}{N_{B_{(s)}^0 \rightarrow J/\psi\eta} \varepsilon_{B_{(s)}^0 \rightarrow J/\psi\eta'} \mathcal{B}(\eta' \rightarrow \eta\pi^+\pi^-) \mathcal{B}(\eta \rightarrow \gamma\gamma)}, \quad (6)$$

$$R_{\psi(2S)} = \frac{N_{B_s^0 \rightarrow \psi(2S)\eta'} \varepsilon_{B_s^0 \rightarrow J/\psi\eta'} \mathcal{B}(J/\psi \rightarrow \mu^+\mu^-)}{N_{B_s^0 \rightarrow J/\psi\eta'} \varepsilon_{B_s^0 \rightarrow \psi(2S)\eta'} \mathcal{B}(\psi(2S) \rightarrow \mu^+\mu^-)}, \quad (7)$$

where N represents the observed yield, ε is the total efficiency and f_s/f_d is the ratio between the probabilities for a b quark to form a B_s^0 and a B^0 meson. Equal values of $f_s/f_d = 0.259 \pm 0.015$ [53–56] at centre-of-mass energies of 7 TeV and 8 TeV are assumed. The branching fractions for η , η' and π^0 decays are taken from Ref. [49]. For the ratio of the $J/\psi \rightarrow \mu^+\mu^-$ and $\psi(2S) \rightarrow \mu^+\mu^-$ branching fractions, the ratio of dielectron branching fractions, 7.57 ± 0.17 [49], is used.

The total efficiency is the product of the geometric acceptance, and the detection, reconstruction, selection and trigger efficiencies. The ratios of efficiencies are determined using simulation. For $R_{(s)}$, the efficiency ratios are further corrected for the small energy-dependent difference in photon reconstruction efficiency between data and simulation.

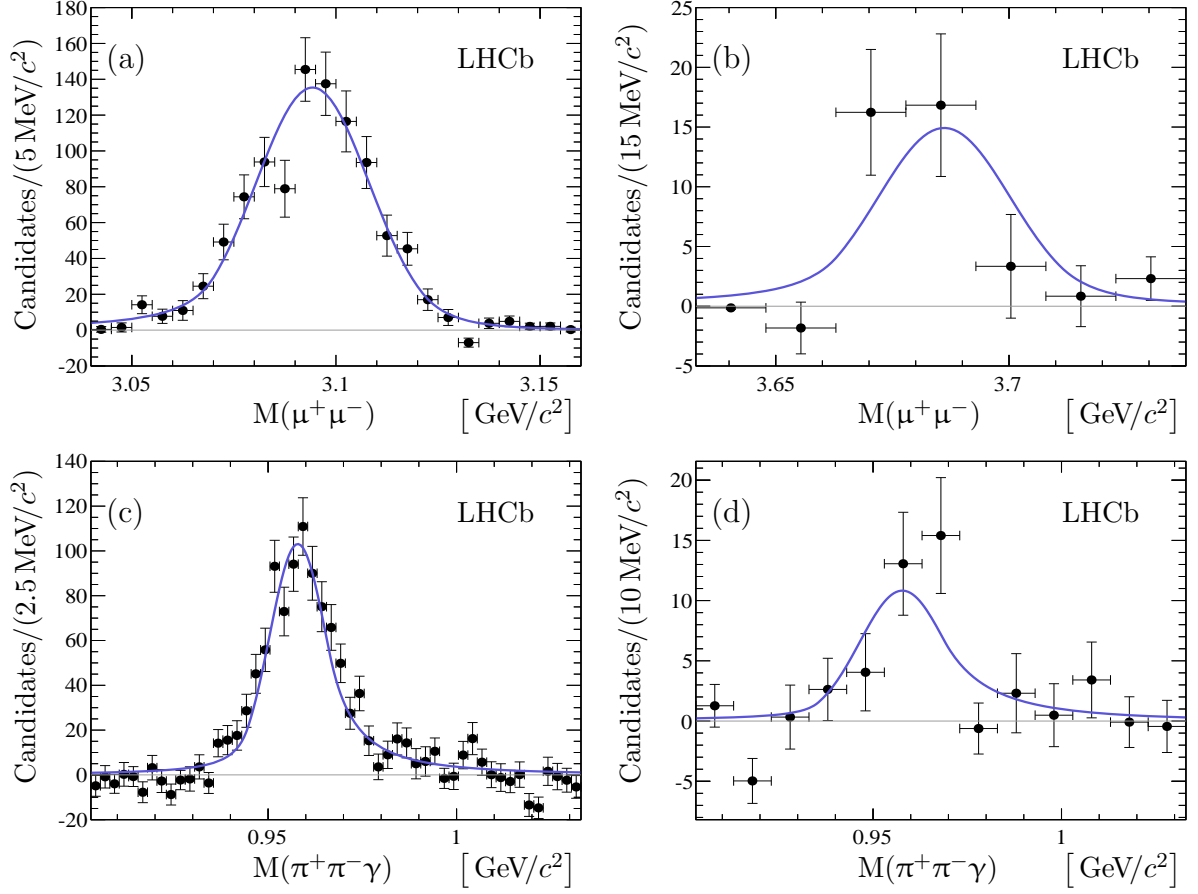


Figure 6: Background subtracted $\psi \rightarrow \mu^+\mu^-$ (a,b) and $\eta' \rightarrow \pi^+\pi^-\gamma$ (c,d) mass distributions in $B_s^0 \rightarrow \psi\eta'$ decays. The figures (a,c) correspond to the J/ψ channel, and the figures (b,d) correspond to the $\psi(2S)$ channel. The solid curves represent the total fit functions.

The photon reconstruction efficiency has been studied using a large sample of $B^+ \rightarrow J/\psi K^{*+}$ decays, followed by $K^{*+} \rightarrow K^+\pi^0$ and $\pi^0 \rightarrow \gamma\gamma$ decays [16, 46, 57, 58]. The correction for the ratios $\epsilon_{B_s^0 \rightarrow J/\psi\eta} / \epsilon_{B_s^0 \rightarrow J/\psi\eta'}$ is estimated to be $(94.9 \pm 2.0)\%$. For the $R_{\eta^{(\prime)}}$ and $R_{\psi(2S)}$ cases no such corrections are required because photon kinematic properties are similar. The ratios of efficiencies are presented in Table 4. The ratio of efficiencies for the ratio $R_{\psi(2S)}$ exceeds the others due to the $p_T(\eta') > 2.5 \text{ GeV}/c$ requirement and the difference in $p_T(\eta')$ spectra between the two channels.

Since the decay products in each of the pairs of channels involved in the ratios have similar kinematic properties, most uncertainties cancel in the ratios, in particular those related to the muon and ψ reconstruction and identification. The remaining systematic uncertainties, except for the one related to the photon reconstruction, are summarised in Table 5 and discussed below.

Systematic uncertainties related to the fit model are estimated using alternative models for the description of the mass distributions. The tested alternatives are first- or second-

Table 4: Ratios of the total efficiencies as defined in Eqs. (5)–(7). The quoted uncertainties are statistical only and reflect the sizes of the simulated samples.

Measured ratio	Efficiency ratio
$R_{\eta'}$	1.096 ± 0.006
R_{η}	1.104 ± 0.006
R_s	1.059 ± 0.006
R	1.052 ± 0.006
$R_{\psi(2S)}$	1.352 ± 0.016

Table 5: Systematic uncertainties (in %) of the ratios of the branching fractions.

Channel	$R_{\eta'}$	R_{η}	R_s	R	$R_{\psi(2S)}$
Photon reconstruction	–	–	2.1	2.1	–
Fit model	2.9	2.9	0.8	2.6	1.2
Data-simulation agreement	2.9	3.7	3.7	3.7	2.9
Trigger	1.1	1.1	1.1	1.1	1.1
Simulation conditions	1.4	1.5	0.8	1.1	0.9
Total	4.5	5.1	4.5	5.2	3.4

degree polynomial functions for the background description, a model with floating mass difference between B^0 and B_s^0 peaks, and a model with Student’s t-distributions for the signal shapes. For the $B_{(s)}^0 \rightarrow J/\psi \eta'$ followed by $\eta' \rightarrow \eta \pi^+ \pi^-$ decays, and $B_{(s)}^0 \rightarrow J/\psi \eta$ decays, an additional model with signal widths fixed to those obtained in simulation is tested. For each alternative fit model, the ratio of event yields is calculated and the systematic uncertainty is determined as the maximum deviation from the ratio obtained with the baseline model. The resulting uncertainties range between 0.8% and 2.9%.

Another important source of systematic uncertainty arises from the potential disagreement between data and simulation in the estimation of efficiencies, apart from those related to π^0 and γ reconstruction. This source is studied by varying the selection criteria, listed in Sect. 3, in ranges that lead to as much as 20% change in the measured signal yields. The agreement is estimated by comparing the efficiency-corrected yields within these variations. The largest deviations range between 2.9% and 3.7% and these values are taken as systematic uncertainties.

To estimate a possible systematic uncertainty related to the knowledge of the B_s^0 production properties, the ratio of efficiencies determined without correcting the B_s^0 transverse momentum and rapidity spectra is compared to the default ratio of efficiencies determined after the corrections. The resulting relative difference is less than 0.2% and is therefore neglected. The trigger is highly efficient in selecting $B_{(s)}^0$ meson decays

with two muons in the final state. For this analysis the dimuon pair is required to be compatible with triggering the event. The trigger efficiency for events with $\psi \rightarrow \mu^+ \mu^-$ produced in beauty hadron decays is studied in data. A systematic uncertainty of 1.1% is assigned based on the comparison of the ratio of trigger efficiencies for samples of $B^+ \rightarrow J/\psi K^+$ and $B^+ \rightarrow \psi(2S)K^+$ decays in data and simulation [59]. The final systematic uncertainty originates from the dependence of the geometric acceptance on the beam crossing angle and the position of the luminosity region. The observed channel-dependent 0.8% – 1.5% differences are taken as systematic uncertainties. The effect of the exclusion of photons that potentially originate from $\pi^0 \rightarrow \gamma\gamma$ candidates is studied by comparing the efficiencies between data and simulation. The difference is found to be negligible. The total uncertainties in Table 5 are obtained by adding the individual independent uncertainties in quadrature.

7 Results and conclusions

The ratios of branching fractions involving $B_{(s)}^0 \rightarrow J/\psi \eta^{(\prime)}$ decays, $R_{\eta^{(\prime)}}$ and $R_{(s)}$, are determined using Eqs. (5) and (6) with the results from Sects. 4, 5 and 6,

$$\begin{aligned} R_{\eta'} &= \frac{\mathcal{B}(B^0 \rightarrow J/\psi \eta')}{\mathcal{B}(B_s^0 \rightarrow J/\psi \eta')} = (2.28 \pm 0.65 \text{ (stat)} \pm 0.10 \text{ (syst)} \pm 0.13 (f_s/f_d)) \times 10^{-2}, \\ R_{\eta} &= \frac{\mathcal{B}(B^0 \rightarrow J/\psi \eta)}{\mathcal{B}(B_s^0 \rightarrow J/\psi \eta)} = (1.85 \pm 0.61 \text{ (stat)} \pm 0.09 \text{ (syst)} \pm 0.11 (f_s/f_d)) \times 10^{-2}, \\ R_s &= \frac{\mathcal{B}(B_s^0 \rightarrow J/\psi \eta')}{\mathcal{B}(B_s^0 \rightarrow J/\psi \eta)} = 0.902 \pm 0.072 \text{ (stat)} \pm 0.041 \text{ (syst)} \pm 0.019 (\mathcal{B}), \\ R &= \frac{\mathcal{B}(B^0 \rightarrow J/\psi \eta')}{\mathcal{B}(B^0 \rightarrow J/\psi \eta)} = 1.111 \pm 0.475 \text{ (stat)} \pm 0.058 \text{ (syst)} \pm 0.023 (\mathcal{B}), \end{aligned}$$

where the third uncertainty is associated with the uncertainty of f_s/f_d for the ratios $R_{\eta^{(\prime)}}$ and the uncertainties of the branching fractions for $\eta^{(\prime)}$ decays for the ratios $R_{(s)}$. The R_s determination is in good agreement with previous results [14, 16] and has better precision.

The ratios $R_{\eta'}$ and R_{η} allow a determination of the mixing angle φ_P using the expressions

$$R_{\eta'} = \left(\frac{\Phi^{\eta'}}{\Phi_s^{\eta'}} \right)^3 \frac{\tan^2 \theta_C}{2} \tan^2 \varphi_P, \quad R_{\eta} = \left(\frac{\Phi^{\eta}}{\Phi_s^{\eta}} \right)^3 \frac{\tan^2 \theta_C}{2} \cot^2 \varphi_P, \quad (8)$$

where θ_C is the Cabibbo angle. These relations are similar to those discussed in Ref. [4]. In comparison with Eq. (2) these expressions are not sensitive to gluonic contributions and have significantly reduced theory uncertainties related to the $B_{(s)} \rightarrow J/\psi$ form-factors. The values for the mixing angle φ_P determined from the ratios $R_{\eta'}$ and R_{η} are $(43.8_{-5.4}^{+3.9})^\circ$ and $(49.4_{-4.5}^{+6.5})^\circ$, respectively. An additional uncertainty of 0.8° comes from the knowledge of f_s/f_d and reduces to 0.1° in the combination of these measurements,

$$\varphi_P|_{R_{\eta^{(\prime)}}} = (46.3 \pm 2.3)^\circ.$$

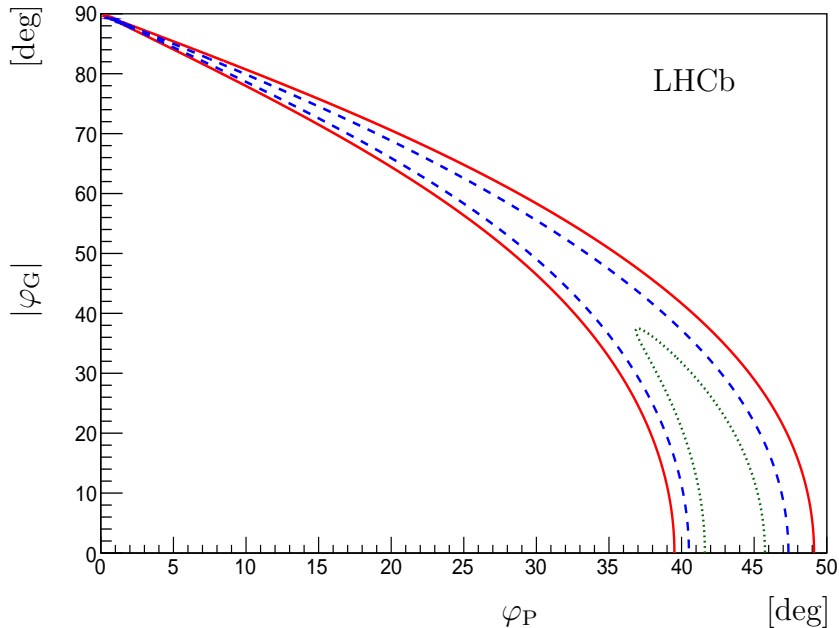


Figure 7: Confidence regions derived from the likelihood function $\mathcal{L}(\varphi_P, |\varphi_G|)$. The contours corresponding to $-2\Delta \ln \mathcal{L} = 2.3, 6.2$ and 11.8 are shown with dotted green, dashed blue and solid red lines.

The measured ratios R and R_s , together with Eqs. (2) and (3), give

$$\tan^4 \varphi_P = 1.26 \pm 0.55, \quad \cos^4 \varphi_G = 1.58 \pm 0.70.$$

The contours of the two-dimensional likelihood function $\mathcal{L}(\varphi_P, |\varphi_G|)$, constructed from Eqs. (2) and (3) are presented in Fig. 7. The estimates for each angle are obtained by treating the other angle as a nuisance parameter and profiling the likelihood with respect to it,

$$\varphi_P|_{R(s)} = (43.5^{+1.4}_{-2.8})^\circ, \quad \varphi_G|_{R(s)} = (0 \pm 24.6)^\circ,$$

where the uncertainties correspond to $\Delta \ln \mathcal{L} = 1/2$ for the profile likelihood. This result does not support a large gluonic contribution in the η' meson. Neglecting the gluonic component, the angle φ_P is determined using Eq. (2) separately from the ratios R and R_s to be $(49.9^{+6.1}_{-11.5})^\circ$ and $(43.4^{+1.4}_{-1.3})^\circ$, respectively. The combination yields

$$\varphi_P|_{R(s), \varphi_G=0} = (43.5^{+1.4}_{-1.3})^\circ,$$

which is consistent with the result from $R_{\eta^{(\prime)}}$. The measured η - η' mixing parameters are in agreement with earlier measurements and have comparable precisions.

The first evidence for the $B_s^0 \rightarrow \psi(2S)\eta'$ decay is found. Using Eq. (7), and combining the results from Sects. 5 and 6, the ratio $R_{\psi(2S)}$ is calculated to be

$$R_{\psi(2S)} = \frac{\mathcal{B}(B_s^0 \rightarrow \psi(2S)\eta')}{\mathcal{B}(B_s^0 \rightarrow J/\psi\eta')} = (38.7 \pm 9.0 \text{ (stat)} \pm 1.3 \text{ (syst)} \pm 0.9(\mathcal{B})) \times 10^{-2},$$

where the first uncertainty is statistical, the second is systematic and the third is due to the limited knowledge of the branching fractions of the J/ψ and $\psi(2S)$ mesons. The measured ratio $R_{\psi(2S)}$ is in agreement with theoretical predictions [60, 61] and similar to other relative decay rates of beauty hadrons to $\psi(2S)$ and J/ψ mesons [46, 59, 62–65].

The reported branching-fraction ratios correspond to the decay-time-integrated rates, while theory predictions usually refer to the branching fractions at the decay time $t = 0$. Due to a sizeable decay width difference in the B_s^0 system [66], the difference can be as large as 10% for $B_s^0 \rightarrow \psi\eta^{(\prime)}$ decays, depending on the decay dynamics [67]. The corresponding change in the angle φ_P can be up to 3° .

In summary, a study of B^0 and B_s^0 meson decays into $J/\psi\eta$ and $J/\psi\eta'$ final states is performed in a data set of proton-proton collisions at centre-of-mass energies of 7 and 8 TeV, collected by the LHCb experiment and corresponding to 3.0 fb^{-1} of integrated luminosity. All four $B_{(s)}^0 \rightarrow J/\psi\eta^{(\prime)}$ decay rates are measured in a single experiment for the first time. The first observation of the decay $B^0 \rightarrow J/\psi\eta'$ and the first evidence for the decay $B_s^0 \rightarrow \psi(2S)\eta'$ are reported. All these results are among the most precise available from a single experiment and contribute to understanding the role of the strong interactions in the internal composition of mesons.

Acknowledgements

We thank A. K. Likhoded for fruitful discussions on $\eta - \eta'$ mixing and for providing us with Eq. (8). We express our gratitude to our colleagues in the CERN accelerator departments for the excellent performance of the LHC. We thank the technical and administrative staff at the LHCb institutes. We acknowledge support from CERN and from the national agencies: CAPES, CNPq, FAPERJ and FINEP (Brazil); NSFC (China); CNRS/IN2P3 (France); BMBF, DFG, HGF and MPG (Germany); SFI (Ireland); INFN (Italy); FOM and NWO (The Netherlands); MNiSW and NCN (Poland); MEN/IFA (Romania); MinES and FANO (Russia); MinECo (Spain); SNSF and SER (Switzerland); NASU (Ukraine); STFC (United Kingdom); NSF (USA). The Tier1 computing centres are supported by IN2P3 (France), KIT and BMBF (Germany), INFN (Italy), NWO and SURF (The Netherlands), PIC (Spain), GridPP (United Kingdom). We are indebted to the communities behind the multiple open source software packages on which we depend. We are also thankful for the computing resources and the access to software R&D tools provided by Yandex LLC (Russia). Individual groups or members have received support from EPLANET, Marie Skłodowska-Curie Actions and ERC (European Union), Conseil général de Haute-Savoie, Labex ENIGMASS and OCEVU, Région Auvergne (France), RFBR (Russia), XuntaGal and GENCAT (Spain), Royal Society and Royal Commission for the Exhibition of 1851 (United Kingdom).

References

- [1] C. Di Donato, G. Ricciardi, and I. Bigi, $\eta - \eta'$ mixing – from electromagnetic transitions to weak decays of charm and beauty hadrons, Phys. Rev. **D85** (2012) 013016, arXiv:1105.3557.
- [2] Y.-D. Tsai, H.-n. Li, and Q. Zhao, η_c mixing effects on charmonium and B meson decays, Phys. Rev. **D85** (2012) 034002, arXiv:1110.6235.
- [3] R. Fleischer, R. Kneijens, and G. Ricciardi, Exploring CP violation and $\eta - \eta'$ mixing with the $B_{(s)}^0 \rightarrow J/\psi \eta^{(\prime)}$ systems, Eur. Phys. J. **C71** (2011) 1798, arXiv:1110.5490.
- [4] A. Datta, H. J. Lipkin, and P. J. O'Donnell, Simple relations for two-body B decays to charmonium and tests for $\eta - \eta'$ mixing, Phys. Lett. **B529** (2002) 93, arXiv:hep-ph/0111336.
- [5] J. L. Rosner, Quark content of neutral mesons, Phys. Rev. **D27** (1983) 1101.
- [6] A. Bramon, R. Escribano, and M. D. Scadron, The $\eta - \eta'$ mixing angle revisited, Eur. Phys. J. **C7** (1999) 271, arXiv:hep-ph/9711229.
- [7] A. Bramon, R. Escribano, and M. D. Scadron, Mixing of $\eta - \eta'$ mesons in J/ψ decays into a vector and a pseudoscalar meson, Phys. Lett. **B403** (1997) 339, arXiv:hep-ph/9703313.
- [8] V. A. Novikov, M. A. Shifman, A. I. Vainshtein, and V. I. Zakharov, A theory of the $J/\psi \rightarrow \eta(\eta')\gamma$ decays, Nucl. Phys. **B165** (1980) 55.
- [9] V. A. Novikov, M. A. Shifman, A. I. Vainshtein, and V. I. Zakharov, η' meson as pseudoscalar gluonium, Phys. Lett. **B86** (1979) 347.
- [10] V. A. Novikov, M. A. Shifman, A. I. Vainshtein, and V. I. Zakharov, In a search for scalar gluonium, Nucl. Phys. **B165** (1980) 67.
- [11] A. L. Kataev, N. V. Krasnikov, and A. A. Pivovarov, The connection between the scales of the gluon and quark worlds in perturbative QCD, Phys. Lett. **B107** (1981) 115.
- [12] A. L. Kataev, N. V. Krasnikov, and A. A. Pivovarov, Two loop calculations for the propagators of gluonic currents, Nucl. Phys. **B198** (1982) 508, arXiv:hep-ph/9612326.
- [13] Belle collaboration, M.-C. Chang *et al.*, Observation of the decay $B^0 \rightarrow J/\psi \eta$, Phys. Rev. Lett. **98** (2007) 131803, arXiv:hep-ex/0609047.
- [14] Belle collaboration, M.-C. Chang *et al.*, Measurement of $B_s^0 \rightarrow J/\psi \eta^{(\prime)}$ and constraint on the $\eta - \eta'$ mixing angle, Phys. Rev. **D85** (2012) 091102, arXiv:1203.3399.

- [15] Belle collaboration, J. Li *et al.*, *First observation of $B_s^0 \rightarrow J/\psi \eta$ and $B_s^0 \rightarrow J/\psi \eta'$* , Phys. Rev. Lett. **108** (2012) 181808, [arXiv:1202.0103](#).
- [16] LHCb collaboration, R. Aaij *et al.*, *Evidence for the decay $B^0 \rightarrow J/\psi \omega$ and measurement of the relative branching fractions of B_s^0 meson decays to $J/\psi \eta$ and $J/\psi \eta'$* , Nucl. Phys. **B867** (2013) 547, [arXiv:1210.2631](#).
- [17] T. Feldmann, P. Kroll, and B. Stech, *Mixing and decay constants of pseudoscalar mesons*, Phys. Rev. **D58** (1998) 114006, [arXiv:hep-ph/9802409](#).
- [18] F.-G. Cao and A. I. Signal, *Two analytical constraints on the $\eta - \eta'$ mixing*, Phys. Rev. **D60** (1999) 114012, [arXiv:hep-ph/9908481](#).
- [19] A. Bramon, R. Escribano, and M. D. Scadron, *Radiative $V \rightarrow P\gamma$ transitions and $\eta - \eta'$ mixing*, Phys. Lett. **B503** (2001) 271, [arXiv:hep-ph/0012049](#).
- [20] B.-W. Xiao and B.-Q. Ma, *Photon-meson transition form-factors of light pseudoscalar mesons*, Phys. Rev. **D71** (2005) 014034, [arXiv:hep-ph/0501160](#).
- [21] R. Escribano and J.-M. Frere, *Study of the $\eta - \eta'$ system in the two mixing angle scheme*, JHEP **06** (2005) 029, [arXiv:hep-ph/0501072](#).
- [22] R. Escribano, *Short study of the $\eta - \eta'$ system in the two mixing angle scheme*, PoS **HEP2005** (2006) 418, [arXiv:hep-ph/0512021](#).
- [23] T. Huang and X.-G. Wu, *Determination of the η and η' mixing angle from the pseudoscalar transition form factors*, Eur. Phys. J. **C50** (2007) 771, [arXiv:hep-ph/0612007](#).
- [24] F. Ambrosino *et al.*, *A global fit to determine the pseudoscalar mixing angle and the gluonium content of the η' meson*, JHEP **07** (2009) 105, [arXiv:0906.3819](#).
- [25] C. E. Thomas, *Composition of the pseudoscalar η and η' mesons*, JHEP **10** (2007) 026, [arXiv:0705.1500](#).
- [26] R. Escribano and J. Nadal, *On the gluon content of the η and η' mesons*, JHEP **05** (2007) 006, [arXiv:hep-ph/0703187](#).
- [27] R. Escribano, *$J/\psi \rightarrow VP$ decays and the quark and gluon content of the η and η'* , Eur. Phys. J. **C65** (2010) 467, [arXiv:0807.4201](#).
- [28] CLEO collaboration, J. Yelton *et al.*, *Absolute branching fraction measurements for exclusive $D_{(s)}$ semileptonic decays*, Phys. Rev. **D80** (2009) 052007, [arXiv:0903.0601](#).
- [29] CLEO collaboration, J. Yelton *et al.*, *Studies of $D^+ \rightarrow \{\eta', \eta, \phi\} e^+ \nu_e$* , Phys. Rev. **D84** (2011) 032001, [arXiv:1011.1195](#).

- [30] B. Bhattacharya and J. L. Rosner, *Decays of charmed mesons to PV final states*, Phys. Rev. **D79** (2009) 034016, [arXiv:0812.3167](#).
- [31] B. Bhattacharya and J. L. Rosner, *Charmed meson decays to two pseudoscalars*, Phys. Rev. **D81** (2010) 014026, [arXiv:0911.2812](#).
- [32] B. Bhattacharya and J. L. Rosner, *Effect of $\eta - \eta'$ mixing on $D \rightarrow PV$ decays*, Phys. Rev. **D82** (2010) 037502, [arXiv:1005.2159](#).
- [33] BaBar collaboration, J. P. Lees *et al.*, *Branching fraction measurements of the color-suppressed decays $\bar{B}^0 \rightarrow D^{*0}\pi^0$, $D^{*0}\eta$, $D^{*0}\omega$, and $D^{*0}\eta'$ and measurement of the polarization in the decay $\bar{B}^0 \rightarrow D^{*0}\omega$* , Phys. Rev. **D84** (2011) 112007, [arXiv:1107.5751](#).
- [34] S. V. Donskov *et al.*, *Measurement of the mixing angle in pseudoscalar meson sector π^- and K^- beams with GAMS-4 π setup*, Eur. Phys. J. **C73** (2013) , [arXiv:1301.6987](#).
- [35] LHCb collaboration, A. A. Alves Jr. *et al.*, *The LHCb detector at the LHC*, JINST **3** (2008) S08005.
- [36] R. Aaij *et al.*, *Performance of the LHCb vertex locator*, JINST **9** (2014) P09007, [arXiv:1405.7808](#).
- [37] R. Arink *et al.*, *Performance of the LHCb outer tracker*, JINST **9** (2014) P01002, [arXiv:1311.3893](#).
- [38] M. Adinolfi *et al.*, *Performance of the LHCb RICH detector at the LHC*, Eur. Phys. J. **C73** (2013) 2431, [arXiv:1211.6759](#).
- [39] A. A. Alves Jr. *et al.*, *Performance of the LHCb muon system*, JINST **8** (2013) P02022, [arXiv:1211.1346](#).
- [40] T. Sjöstrand, S. Mrenna, and P. Skands, *PYTHIA 6.4 physics and manual*, JHEP **05** (2006) 026, [arXiv:hep-ph/0603175](#); T. Sjöstrand, S. Mrenna, and P. Skands, *A brief introduction to PYTHIA 8.1*, Comput. Phys. Commun. **178** (2008) 852, [arXiv:0710.3820](#).
- [41] I. Belyaev *et al.*, *Handling of the generation of primary events in GAUSS, the LHCb simulation framework*, Nuclear Science Symposium Conference Record (NSS/MIC) **IEEE** (2010) 1155.
- [42] D. J. Lange, *The EVTGEN particle decay simulation package*, Nucl. Instrum. Meth. **A462** (2001) 152.
- [43] P. Golonka and Z. Was, *PHOTOS Monte Carlo: A precision tool for QED corrections in Z and W decays*, Eur. Phys. J. **C45** (2006) 97, [arXiv:hep-ph/0506026](#).

- [44] Geant4 collaboration, J. Allison *et al.*, *GEANT4 developments and applications*, IEEE Trans. Nucl. Sci. **53** (2006) 270; Geant4 collaboration, S. Agostinelli *et al.*, *GEANT4: A simulation toolkit*, Nucl. Instrum. Meth. **A506** (2003) 250.
- [45] M. Clemencic *et al.*, *The LHCb simulation application, GAUSS: Design, evolution and experience*, J. Phys. Conf. Ser. **331** (2011) 032023.
- [46] LHCb collaboration, R. Aaij *et al.*, *Observations of $B_s^0 \rightarrow \psi(2S)\eta$ and $B_{(s)}^0 \rightarrow \psi(2S)\pi^+\pi^-$ decays*, Nucl. Phys. **B871** (2013) 403, [arXiv:1302.6354](#).
- [47] F. Archilli *et al.*, *Performance of the muon identification at LHCb*, JINST **8** (2013) P10020, [arXiv:1306.0249](#).
- [48] LHCb collaboration, R. Aaij *et al.*, *Measurement of the ratio of prompt χ_c to J/ψ production in pp collisions at $\sqrt{s} = 7$ TeV*, Phys. Lett. **B718** (2012) 431, [arXiv:1204.1462](#).
- [49] Particle Data Group, K. A. Olive *et al.*, *Review of particle physics*, Chin. Phys. **C38** (2014) 090001.
- [50] W. D. Hulsbergen, *Decay chain fitting with a Kalman filter*, Nucl. Instrum. Meth. **A552** (2005) 566, [arXiv:physics/0503191](#).
- [51] LHCb collaboration, R. Aaij *et al.*, *Observation of J/ψ -pair production in pp collisions at $\sqrt{s} = 7$ TeV*, Phys. Lett. **B707** (2012) 52, [arXiv:1109.0963](#).
- [52] M. Pivk and F. R. Le Diberder, *sPlot: A statistical tool to unfold data distributions*, Nucl. Instrum. Meth. **A555** (2005) 356, [arXiv:physics/0402083](#).
- [53] LHCb collaboration, *Updated average f_s/f_d b-hadron production fraction ratio for 7 TeV pp collisions*, LHCb-CONF-2013-011.
- [54] LHCb collaboration, R. Aaij *et al.*, *Measurement of b hadron production fractions in 7 TeV pp collisions*, Phys. Rev. **D85** (2012) 032008, [arXiv:1111.2357](#).
- [55] LHCb collaboration, R. Aaij *et al.*, *Determination of f_s/f_d for 7 TeV pp collisions and measurement of the $B^0 \rightarrow D^-K^+$ branching fraction*, Phys. Rev. Lett. **107** (2011) 211801, [arXiv:1106.4435](#).
- [56] LHCb collaboration, R. Aaij *et al.*, *Measurement of the fragmentation fraction ratio f_s/f_d and its dependence on B meson kinematics*, JHEP **04** (2013) 001, [arXiv:1301.5286](#).
- [57] LHCb collaboration, R. Aaij *et al.*, *Observation of $B_s^0 \rightarrow \chi_{c1}\phi$ decay and study of $B^0 \rightarrow \chi_{c1,2}K^{*0}$ decays*, Nucl. Phys. **B874** (2013) 663, [arXiv:1305.6511](#).
- [58] LHCb collaboration, R. Aaij *et al.*, *Evidence for the decay $X(3872) \rightarrow \psi(2S)\gamma$* , Nucl. Phys. **B886** (2014) 665, [arXiv:1404.0275](#).

- [59] LHCb collaboration, R. Aaij *et al.*, *Measurement of relative branching fractions of B decays to $\psi(2S)$ and J/ψ mesons*, Eur. Phys. J. **C72** (2012) 2118, [arXiv:1205.0918](#).
- [60] P. Colangelo, F. De Fazio, and W. Wang, *Nonleptonic B_s^0 to charmonium decays: analyses in pursuit of determining the weak phase β_s* , Phys. Rev. **D83** (2011) 094027, [arXiv:1009.4612](#).
- [61] R. N. Faustov and V. O. Galkin, *Rare B_s^0 decays in the relativistic quark model*, Eur. Phys. J. **C73** (2013) 2593, [arXiv:1309.2160](#).
- [62] CDF collaboration, F. Abe *et al.*, *Observation of $B^+ \rightarrow \psi(2S)K^+$ and $B^0 \rightarrow \psi(2S)K^{*0}(892)$ decays and measurements of B meson branching fractions into J/ψ and $\psi(2S)$ final states*, Phys. Rev. **D58** (1998) 072001, [arXiv:hep-ex/9803013](#).
- [63] CDF collaboration, A. Abulencia *et al.*, *Observation of $B_s^0 \rightarrow \psi(2S)\phi$ and measurement of ratio of branching fractions $\mathcal{B}(B_s^0 \rightarrow \psi(2S)\phi)/\mathcal{B}(B_s^0 \rightarrow J/\psi\phi)$* , Phys. Rev. Lett. **96** (2006) 231801, [arXiv:hep-ex/0602005](#).
- [64] D0 collaboration, V. M. Abazov *et al.*, *Relative rates of B meson decays into $\psi(2S)$ and J/ψ mesons*, Phys. Rev. **D79** (2009) 111102, [arXiv:0805.2576](#).
- [65] LHCb collaboration, R. Aaij *et al.*, *Observation of the decay $B_c^+ \rightarrow \psi(2S)\pi^+$* , Phys. Rev. **D87** (2013) 071103(R), [arXiv:1303.1737](#).
- [66] LHCb collaboration, R. Aaij *et al.*, *Measurement of CP violation and the B_s^0 meson decay width difference with $B_s^0 \rightarrow J/\psi K^+K^-$ and $B_s^0 \rightarrow J/\psi \pi^-\pi^-$ decays*, Phys. Rev. **D87** (2013) 112010, [arXiv:1304.2600](#).
- [67] K. De Bruyn *et al.*, *Branching ratio measurements of B_s^0 decays*, Phys. Rev. **D86** (2012) 014027, [arXiv:1204.1735](#).

LHCb collaboration

R. Aaij⁴¹, B. Adeva³⁷, M. Adinolfi⁴⁶, A. Affolder⁵², Z. Ajaltouni⁵, S. Akar⁶, J. Albrecht⁹, F. Alessio³⁸, M. Alexander⁵¹, S. Ali⁴¹, G. Alkhazov³⁰, P. Alvarez Cartelle³⁷, A.A. Alves Jr^{25,38}, S. Amato², S. Amerio²², Y. Amhis⁷, L. An³, L. Anderlini^{17,g}, J. Anderson⁴⁰, R. Andreassen⁵⁷, M. Andreotti^{16,f}, J.E. Andrews⁵⁸, R.B. Appleby⁵⁴, O. Aquines Gutierrez¹⁰, F. Archilli³⁸, A. Artamonov³⁵, M. Artuso⁵⁹, E. Aslanides⁶, G. Auriemma^{25,n}, M. Baalouch⁵, S. Bachmann¹¹, J.J. Back⁴⁸, A. Badalov³⁶, C. Baesso⁶⁰, W. Baldini¹⁶, R.J. Barlow⁵⁴, C. Barschel³⁸, S. Barsuk⁷, W. Barter⁴⁷, V. Batozskaya²⁸, V. Battista³⁹, A. Bay³⁹, L. Beaucourt⁴, J. Beddow⁵¹, F. Bedeschi²³, I. Bediaga¹, S. Belogurov³¹, K. Belous³⁵, I. Belyaev³¹, E. Ben-Haim⁸, G. Bencivenni¹⁸, S. Benson³⁸, J. Benton⁴⁶, A. Berezhnoy³², R. Bernet⁴⁰, AB Bertolin²², M.-O. Bettler⁴⁷, M. van Beuzekom⁴¹, A. Bien¹¹, S. Bifani⁴⁵, T. Bird⁵⁴, A. Bizzeti^{17,i}, P.M. Bjørnstad⁵⁴, T. Blake⁴⁸, F. Blanc³⁹, J. Blouw¹⁰, S. Blusk⁵⁹, V. Bocci²⁵, A. Bondar³⁴, N. Bondar^{30,38}, W. Bonivento¹⁵, S. Borghi⁵⁴, A. Borgia⁵⁹, M. Borsato⁷, T.J.V. Bowcock⁵², E. Bowen⁴⁰, C. Bozzi¹⁶, D. Brett⁵⁴, M. Britsch¹⁰, T. Britton⁵⁹, J. Brodzicka⁵⁴, N.H. Brook⁴⁶, H. Brown⁵², A. Bursche⁴⁰, J. Buytaert³⁸, S. Cadeddu¹⁵, R. Calabrese^{16,f}, M. Calvi^{20,k}, M. Calvo Gomez^{36,p}, P. Campana¹⁸, D. Campora Perez³⁸, L. Capriotti⁵⁴, A. Carbone^{14,d}, G. Carboni^{24,l}, R. Cardinale^{19,38,j}, A. Cardini¹⁵, L. Carson⁵⁰, K. Carvalho Akiba^{2,38}, RCM Casanova Mohr³⁶, G. Casse⁵², L. Cassina^{20,k}, L. Castillo Garcia³⁸, M. Cattaneo³⁸, Ch. Cauet⁹, R. Cenci^{23,t}, M. Charles⁸, Ph. Charpentier³⁸, M. Chefdeville⁴, S. Chen⁵⁴, S.-F. Cheung⁵⁵, N. Chiapolini⁴⁰, M. Chrzaszcz^{40,26}, X. Cid Vidal³⁸, G. Ciezarek⁴¹, P.E.L. Clarke⁵⁰, M. Clemencic³⁸, H.V. Cliff⁴⁷, J. Closier³⁸, V. Coco³⁸, J. Cogan⁶, E. Cogneras⁵, V. Cogoni¹⁵, L. Cojocariu²⁹, G. Collazuol²², P. Collins³⁸, A. Comerma-Montells¹¹, A. Contu^{15,38}, A. Cook⁴⁶, M. Coombes⁴⁶, S. Coquereau⁸, G. Corti³⁸, M. Corvo^{16,f}, I. Counts⁵⁶, B. Couturier³⁸, G.A. Cowan⁵⁰, D.C. Craik⁴⁸, A.C. Crocombe⁴⁸, M. Cruz Torres⁶⁰, S. Cunliffe⁵³, R. Currie⁵³, C. D'Ambrosio³⁸, J. Dalseno⁴⁶, P. David⁸, P.N.Y. David⁴¹, A. Davis⁵⁷, K. De Bruyn⁴¹, S. De Capua⁵⁴, M. De Cian¹¹, J.M. De Miranda¹, L. De Paula², W. De Silva⁵⁷, P. De Simone¹⁸, C.-T. Dean⁵¹, D. Decamp⁴, M. Deckenhoff⁹, L. Del Buono⁸, N. Déleage⁴, D. Derkach⁵⁵, O. Deschamps⁵, F. Dettori³⁸, A. Di Canto³⁸, H. Dijkstra³⁸, S. Donleavy⁵², F. Dordei¹¹, M. Dorigo³⁹, A. Dosil Suárez³⁷, D. Dossett⁴⁸, A. Dovbnya⁴³, K. Dreimanis⁵², G. Dujany⁵⁴, F. Dupertuis³⁹, P. Durante³⁸, R. Dzhelyadin³⁵, A. Dziurda²⁶, A. Dzyuba³⁰, S. Easo^{49,38}, U. Egede⁵³, V. Egorychev³¹, S. Eidelman³⁴, S. Eisenhardt⁵⁰, U. Eitschberger⁹, R. Ekelhof⁹, L. Eklund⁵¹, I. El Rifai⁵, Ch. Elsasser⁴⁰, S. Ely⁵⁹, S. Esen¹¹, H.-M. Evans⁴⁷, T. Evans⁵⁵, A. Falabella¹⁴, C. Färber¹¹, C. Farinelli⁴¹, N. Farley⁴⁵, S. Farry⁵², R. Fay⁵², D. Ferguson⁵⁰, V. Fernandez Albor³⁷, F. Ferreira Rodrigues¹, M. Ferro-Luzzi³⁸, S. Filippov³³, M. Fiore^{16,f}, M. Fiorini^{16,f}, M. Firlej²⁷, C. Fitzpatrick³⁹, T. Fiutowski²⁷, P. Fol⁵³, M. Fontana¹⁰, F. Fontanelli^{19,j}, R. Forty³⁸, O. Francisco², M. Frank³⁸, C. Frei³⁸, M. Frosini^{17,g}, J. Fu^{21,38}, E. Furfaro^{24,l}, A. Gallas Torreira³⁷, D. Galli^{14,d}, S. Gallorini^{22,38}, S. Gambetta^{19,j}, M. Gandelman², P. Gandini⁵⁹, Y. Gao³, J. García Pardiñas³⁷, J. Garofoli⁵⁹, J. Garra Tico⁴⁷, L. Garrido³⁶, D. Gascon³⁶, C. Gaspar³⁸, U. Gastaldi¹⁶, R. Gauld⁵⁵, L. Gavardi⁹, G. Gazzoni⁵, A. Geraci^{21,v}, E. Gersabeck¹¹, M. Gersabeck⁵⁴, T. Gershon⁴⁸, Ph. Ghez⁴, A. Gianelle²², S. Giani³⁹, V. Gibson⁴⁷, L. Giubega²⁹, V.V. Gligorov³⁸, C. Göbel⁶⁰, D. Golubkov³¹, A. Golutvin^{53,31,38}, A. Gomes^{1,a}, C. Gotti^{20,k}, M. Grabalosa Gándara⁵, R. Graciani Diaz³⁶, L.A. Granado Cardoso³⁸, E. Graugés³⁶, E. Graverini⁴⁰, G. Graziani¹⁷, A. Grecu²⁹, E. Greening⁵⁵, S. Gregson⁴⁷, P. Griffith⁴⁵, L. Grillo¹¹, O. Grünberg⁶³, B. Gui⁵⁹, E. Gushchin³³, Yu. Guz^{35,38}, T. Gys³⁸, C. Hadjivasiliou⁵⁹, G. Haefeli³⁹, C. Haen³⁸, S.C. Haines⁴⁷, S. Hall⁵³,

B. Hamilton⁵⁸, T. Hampson⁴⁶, X. Han¹¹, S. Hansmann-Menzemer¹¹, N. Harnew⁵⁵,
 S.T. Harnew⁴⁶, J. Harrison⁵⁴, J. He³⁸, T. Head³⁹, V. Heijne⁴¹, K. Hennessy⁵², P. Henrard⁵,
 L. Henry⁸, J.A. Hernando Morata³⁷, E. van Herwijnen³⁸, M. Heß⁶³, A. Hicheur², D. Hill⁵⁵,
 M. Hoballah⁵, C. Hombach⁵⁴, W. Hulsbergen⁴¹, N. Hussain⁵⁵, D. Hutchcroft⁵², D. Hynds⁵¹,
 M. Idzik²⁷, P. Ilten⁵⁶, R. Jacobsson³⁸, A. Jaeger¹¹, J. Jalocha⁵⁵, E. Jans⁴¹, P. Jatón³⁹,
 A. Jawahery⁵⁸, F. Jing³, M. John⁵⁵, D. Johnson³⁸, C.R. Jones⁴⁷, C. Joram³⁸, B. Jost³⁸,
 N. Jurik⁵⁹, S. Kandybei⁴³, W. Kanso⁶, M. Karacson³⁸, T.M. Karbach³⁸, S. Karodia⁵¹,
 M. Kelsey⁵⁹, I.R. Kenyon⁴⁵, T. Ketel⁴², B. Khanji^{20,38,k}, C. Khurewathanakul³⁹, S. Klaver⁵⁴,
 K. Klimaszewski²⁸, O. Kochebina⁷, M. Kolpin¹¹, I. Komarov³⁹, R.F. Koopman⁴²,
 P. Koppenburg^{41,38}, M. Korolev³², L. Kravchuk³³, K. Kreplin¹¹, M. Kreps⁴⁸, G. Krocker¹¹,
 P. Krokovny³⁴, F. Kruse⁹, W. Kucewicz^{26,o}, M. Kucharczyk^{20,26,k}, V. Kudryavtsev³⁴,
 K. Kurek²⁸, T. Kvaratskheliya³¹, V.N. La Thi³⁹, D. Lacarrere³⁸, G. Lafferty⁵⁴, A. Lai¹⁵,
 D. Lambert⁵⁰, R.W. Lambert⁴², G. Lanfranchi¹⁸, C. Langenbruch⁴⁸, B. Langhans³⁸,
 T. Latham⁴⁸, C. Lazzeroni⁴⁵, R. Le Gac⁶, J. van Leerdam⁴¹, J.-P. Lees⁴, R. Lefèvre⁵,
 A. Leflat³², J. Lefrançois⁷, S. Leo²³, O. Leroy⁶, T. Lesiak²⁶, B. Leverington¹¹, Y. Li⁷,
 T. Likhomanenko⁶⁴, M. Liles⁵², R. Lindner³⁸, C. Linn³⁸, F. Lionetto⁴⁰, B. Liu¹⁵, S. Lohn³⁸,
 I. Longstaff⁵¹, J.H. Lopes², P. Lowdon⁴⁰, D. Lucchesi^{22,r}, H. Luo⁵⁰, A. Lupato²², E. Luppi^{16,f},
 O. Lupton⁵⁵, F. Machefert⁷, I.V. Machikhiliyan³¹, F. Maciuc²⁹, O. Maev³⁰, S. Malde⁵⁵,
 A. Malinin⁶⁴, G. Manca^{15,e}, G. Mancinelli⁶, A. Mapelli³⁸, J. Maratas⁵, J.F. Marchand⁴,
 U. Marconi¹⁴, C. Marin Benito³⁶, P. Marino^{23,t}, R. Märki³⁹, J. Marks¹¹, G. Martellotti²⁵,
 A. Martín Sánchez⁷, M. Martinelli³⁹, D. Martinez Santos^{42,38}, F. Martinez Vidal⁶⁵,
 D. Martins Tostes², A. Massafferri¹, R. Matev³⁸, Z. Mathe³⁸, C. Matteuzzi²⁰, A. Mazurov⁴⁵,
 M. McCann⁵³, J. McCarthy⁴⁵, A. McNab⁵⁴, R. McNulty¹², B. McSkelly⁵², B. Meadows⁵⁷,
 F. Meier⁹, M. Meissner¹¹, M. Merk⁴¹, D.A. Milanes⁶², M.-N. Minard⁴, N. Moggi¹⁴,
 J. Molina Rodriguez⁶⁰, S. Monteil⁵, M. Morandin²², P. Morawski²⁷, A. Mordà⁶, M.J. Morello^{23,t},
 J. Moron²⁷, A.-B. Morris⁵⁰, R. Mountain⁵⁹, F. Muheim⁵⁰, K. Müller⁴⁰, M. Mussini¹⁴,
 B. Muster³⁹, P. Naik⁴⁶, T. Nakada³⁹, R. Nandakumar⁴⁹, I. Nasteva², M. Needham⁵⁰, N. Neri²¹,
 S. Neubert³⁸, N. Neufeld³⁸, M. Neuner¹¹, A.D. Nguyen³⁹, T.D. Nguyen³⁹, C. Nguyen-Mau^{39,q},
 M. Nicol⁷, V. Niess⁵, R. Niet⁹, N. Nikitin³², T. Nikodem¹¹, A. Novoselov³⁵, D.P. O’Hanlon⁴⁸,
 A. Oblakowska-Mucha^{27,38}, V. Obraztsov³⁵, S. Oggero⁴¹, S. Ogilvy⁵¹, O. Okhrimenko⁴⁴,
 R. Oldeman^{15,e}, C.J.G. Onderwater⁶⁶, M. Orlandea²⁹, J.M. Otalora Goicochea², A. Otto³⁸,
 P. Owen⁵³, A. Oyanguren⁶⁵, B.K. Pal⁵⁹, A. Palano^{13,c}, F. Palombo^{21,u}, M. Palutan¹⁸,
 J. Panman³⁸, A. Papanestis^{49,38}, M. Pappagallo⁵¹, L.L. Pappalardo^{16,f}, C. Parkes⁵⁴,
 C.J. Parkinson^{9,45}, G. Passaleva¹⁷, G.D. Patel⁵², M. Patel⁵³, C. Patrignani^{19,j}, A. Pearce⁵⁴,
 A. Pellegrino⁴¹, G. Penso^{25,m}, M. Pepe Altarelli³⁸, S. Perazzini^{14,d}, P. Perret⁵, M. Perrin-Terrin⁶,
 L. Pescatore⁴⁵, E. Pesen⁶⁷, K. Petridis⁵³, A. Petrolini^{19,j}, E. Picatoste Olloqui³⁶, B. Pietrzyk⁴,
 T. Pilar⁴⁸, D. Pinci²⁵, A. Pistone¹⁹, S. Playfer⁵⁰, M. Plo Casasus³⁷, F. Polci⁸, S. Polikarpov³¹,
 A. Poluektov^{48,34}, I. Polyakov³¹, E. Polcarpo², A. Popov³⁵, D. Popov¹⁰, B. Popovici²⁹,
 C. Potterat², E. Price⁴⁶, J.D. Price⁵², J. Prisciandaro³⁹, A. Pritchard⁵², C. Prouve⁴⁶,
 V. Pugatch⁴⁴, A. Puig Navarro³⁹, G. Punzi^{23,s}, W. Qian⁴, B. Rachwal²⁶, J.H. Rademacker⁴⁶,
 B. Rakotomiarmanana³⁹, M. Rama¹⁸, M.S. Rangel², I. Raniuk⁴³, N. Rauschmayr³⁸,
 G. Raven⁴², F. Redi⁵³, S. Reichert⁵⁴, M.M. Reid⁴⁸, A.C. dos Reis¹, S. Ricciardi⁴⁹, S. Richards⁴⁶,
 M. Rihl³⁸, K. Rinnert⁵², V. Rives Molina³⁶, P. Robbe⁷, A.B. Rodrigues¹, E. Rodrigues⁵⁴,
 P. Rodriguez Perez⁵⁴, S. Roiser³⁸, V. Romanovsky³⁵, A. Romero Vidal³⁷, M. Rotondo²²,
 J. Rouvinet³⁹, T. Ruf³⁸, H. Ruiz³⁶, P. Ruiz Valls⁶⁵, J.J. Saborido Silva³⁷, N. Sagidova³⁰,
 P. Sail⁵¹, B. Saitta^{15,e}, V. Salustino Guimaraes², C. Sanchez Mayordomo⁶⁵,

B. Sanmartin Sedes³⁷, R. Santacesaria²⁵, C. Santamarina Rios³⁷, E. Santovetti^{24,l}, A. Sarti^{18,m}, C. Satriano^{25,n}, A. Satta²⁴, D.M. Saunders⁴⁶, D. Savrina^{31,32}, M. Schiller³⁸, H. Schindler³⁸, M. Schlupp⁹, M. Schmelling¹⁰, B. Schmidt³⁸, O. Schneider³⁹, A. Schopper³⁸, M.-H. Schune⁷, R. Schwemmer³⁸, B. Sciascia¹⁸, A. Sciubba^{25,m}, A. Semennikov³¹, I. Sepp⁵³, N. Serra⁴⁰, J. Serrano⁶, L. Sestini²², P. Seyfert¹¹, M. Shapkin³⁵, I. Shapoval^{16,43,f}, Y. Shcheglov³⁰, T. Shears⁵², L. Shekhtman³⁴, V. Shevchenko⁶⁴, A. Shires⁹, R. Silva Coutinho⁴⁸, G. Simi²², M. Sirendi⁴⁷, N. Skidmore⁴⁶, I. Skillicorn⁵¹, T. Skwarnicki⁵⁹, N.A. Smith⁵², E. Smith^{55,49}, E. Smith⁵³, J. Smith⁴⁷, M. Smith⁵⁴, H. Snoek⁴¹, M.D. Sokoloff⁵⁷, F.J.P. Soler⁵¹, F. Soomro³⁹, D. Souza⁴⁶, B. Souza De Paula², B. Spaan⁹, P. Spradlin⁵¹, S. Sridharan³⁸, F. Stagni³⁸, M. Stahl¹¹, S. Stahl¹¹, O. Steinkamp⁴⁰, O. Stenyakin³⁵, S. Stevenson⁵⁵, S. Stoica²⁹, S. Stone⁵⁹, B. Storaci⁴⁰, S. Stracka^{23,t}, M. Straticiu²⁹, U. Straumann⁴⁰, R. Stroili²², L. Sun⁵⁷, W. Sutcliffe⁵³, K. Swientek²⁷, S. Swientek⁹, V. Syropoulos⁴², M. Szczekowski²⁸, P. Szczypka^{39,38}, T. Szumlak²⁷, S. T'Jampens⁴, M. Teklishyn⁷, G. Tellarini^{16,f}, F. Teubert³⁸, C. Thomas⁵⁵, E. Thomas³⁸, J. van Tilburg⁴¹, V. Tisserand⁴, M. Tobin³⁹, J. Todd⁵⁷, S. Tol⁴², L. Tomassetti^{16,f}, D. Tonelli³⁸, S. Topp-Joergensen⁵⁵, N. Torr⁵⁵, E. Tournefier⁴, S. Tourneur³⁹, M.T. Tran³⁹, M. Tresch⁴⁰, A. Trisovic³⁸, A. Tsaregorodtsev⁶, P. Tsopelas⁴¹, N. Tuning⁴¹, M. Ubeda Garcia³⁸, A. Ukleja²⁸, A. Ustyuzhanin⁶⁴, U. Uwer¹¹, C. Vacca¹⁵, V. Vagnoni¹⁴, G. Valenti¹⁴, A. Vallier⁷, R. Vazquez Gomez¹⁸, P. Vazquez Regueiro³⁷, C. Vázquez Sierra³⁷, S. Vecchi¹⁶, J.J. Velthuis⁴⁶, M. Veltri^{17,h}, G. Veneziano³⁹, M. Vesterinen¹¹, B. Viaud⁷, D. Vieira², M. Vieites Diaz³⁷, X. Vilasis-Cardona^{36,p}, A. Vollhardt⁴⁰, D. Volyanskyy¹⁰, D. Voong⁴⁶, A. Vorobyev³⁰, V. Vorobyev³⁴, C. Voß⁶³, J.A. de Vries⁴¹, R. Waldi⁶³, C. Wallace⁴⁸, R. Wallace¹², J. Walsh²³, S. Wandernoth¹¹, J. Wang⁵⁹, D.R. Ward⁴⁷, N.K. Watson⁴⁵, D. Websdale⁵³, M. Whitehead⁴⁸, D. Wiedner¹¹, G. Wilkinson^{55,38}, M. Wilkinson⁵⁹, M.P. Williams⁴⁵, M. Williams⁵⁶, H.W. Wilschut⁶⁶, F.F. Wilson⁴⁹, J. Wimberley⁵⁸, J. Wishahi⁹, W. Wislicki²⁸, M. Witek²⁶, G. Wormser⁷, S.A. Wotton⁴⁷, S. Wright⁴⁷, K. Wyllie³⁸, Y. Xie⁶¹, Z. Xing⁵⁹, Z. Xu³⁹, Z. Yang³, X. Yuan³, O. Yushchenko³⁵, M. Zangoli¹⁴, M. Zavertyaev^{10,b}, L. Zhang³, W.C. Zhang¹², Y. Zhang³, A. Zhelezov¹¹, A. Zhokhov³¹, L. Zhong³.

¹ Centro Brasileiro de Pesquisas Físicas (CBPF), Rio de Janeiro, Brazil

² Universidade Federal do Rio de Janeiro (UFRJ), Rio de Janeiro, Brazil

³ Center for High Energy Physics, Tsinghua University, Beijing, China

⁴ LAPP, Université de Savoie, CNRS/IN2P3, Annecy-Le-Vieux, France

⁵ Clermont Université, Université Blaise Pascal, CNRS/IN2P3, LPC, Clermont-Ferrand, France

⁶ CPPM, Aix-Marseille Université, CNRS/IN2P3, Marseille, France

⁷ LAL, Université Paris-Sud, CNRS/IN2P3, Orsay, France

⁸ LPNHE, Université Pierre et Marie Curie, Université Paris Diderot, CNRS/IN2P3, Paris, France

⁹ Fakultät Physik, Technische Universität Dortmund, Dortmund, Germany

¹⁰ Max-Planck-Institut für Kernphysik (MPIK), Heidelberg, Germany

¹¹ Physikalisches Institut, Ruprecht-Karls-Universität Heidelberg, Heidelberg, Germany

¹² School of Physics, University College Dublin, Dublin, Ireland

¹³ Sezione INFN di Bari, Bari, Italy

¹⁴ Sezione INFN di Bologna, Bologna, Italy

¹⁵ Sezione INFN di Cagliari, Cagliari, Italy

¹⁶ Sezione INFN di Ferrara, Ferrara, Italy

¹⁷ Sezione INFN di Firenze, Firenze, Italy

¹⁸ Laboratori Nazionali dell'INFN di Frascati, Frascati, Italy

¹⁹ Sezione INFN di Genova, Genova, Italy

²⁰ Sezione INFN di Milano Bicocca, Milano, Italy

²¹ Sezione INFN di Milano, Milano, Italy

- ²² *Sezione INFN di Padova, Padova, Italy*
- ²³ *Sezione INFN di Pisa, Pisa, Italy*
- ²⁴ *Sezione INFN di Roma Tor Vergata, Roma, Italy*
- ²⁵ *Sezione INFN di Roma La Sapienza, Roma, Italy*
- ²⁶ *Henryk Niewodniczanski Institute of Nuclear Physics Polish Academy of Sciences, Kraków, Poland*
- ²⁷ *AGH - University of Science and Technology, Faculty of Physics and Applied Computer Science, Kraków, Poland*
- ²⁸ *National Center for Nuclear Research (NCBJ), Warsaw, Poland*
- ²⁹ *Horia Hulubei National Institute of Physics and Nuclear Engineering, Bucharest-Magurele, Romania*
- ³⁰ *Petersburg Nuclear Physics Institute (PNPI), Gatchina, Russia*
- ³¹ *Institute of Theoretical and Experimental Physics (ITEP), Moscow, Russia*
- ³² *Institute of Nuclear Physics, Moscow State University (SINP MSU), Moscow, Russia*
- ³³ *Institute for Nuclear Research of the Russian Academy of Sciences (INR RAN), Moscow, Russia*
- ³⁴ *Budker Institute of Nuclear Physics (SB RAS) and Novosibirsk State University, Novosibirsk, Russia*
- ³⁵ *Institute for High Energy Physics (IHEP), Protvino, Russia*
- ³⁶ *Universitat de Barcelona, Barcelona, Spain*
- ³⁷ *Universidad de Santiago de Compostela, Santiago de Compostela, Spain*
- ³⁸ *European Organization for Nuclear Research (CERN), Geneva, Switzerland*
- ³⁹ *Ecole Polytechnique Fédérale de Lausanne (EPFL), Lausanne, Switzerland*
- ⁴⁰ *Physik-Institut, Universität Zürich, Zürich, Switzerland*
- ⁴¹ *Nikhef National Institute for Subatomic Physics, Amsterdam, The Netherlands*
- ⁴² *Nikhef National Institute for Subatomic Physics and VU University Amsterdam, Amsterdam, The Netherlands*
- ⁴³ *NSC Kharkiv Institute of Physics and Technology (NSC KIPT), Kharkiv, Ukraine*
- ⁴⁴ *Institute for Nuclear Research of the National Academy of Sciences (KINR), Kyiv, Ukraine*
- ⁴⁵ *University of Birmingham, Birmingham, United Kingdom*
- ⁴⁶ *H.H. Wills Physics Laboratory, University of Bristol, Bristol, United Kingdom*
- ⁴⁷ *Cavendish Laboratory, University of Cambridge, Cambridge, United Kingdom*
- ⁴⁸ *Department of Physics, University of Warwick, Coventry, United Kingdom*
- ⁴⁹ *STFC Rutherford Appleton Laboratory, Didcot, United Kingdom*
- ⁵⁰ *School of Physics and Astronomy, University of Edinburgh, Edinburgh, United Kingdom*
- ⁵¹ *School of Physics and Astronomy, University of Glasgow, Glasgow, United Kingdom*
- ⁵² *Oliver Lodge Laboratory, University of Liverpool, Liverpool, United Kingdom*
- ⁵³ *Imperial College London, London, United Kingdom*
- ⁵⁴ *School of Physics and Astronomy, University of Manchester, Manchester, United Kingdom*
- ⁵⁵ *Department of Physics, University of Oxford, Oxford, United Kingdom*
- ⁵⁶ *Massachusetts Institute of Technology, Cambridge, MA, United States*
- ⁵⁷ *University of Cincinnati, Cincinnati, OH, United States*
- ⁵⁸ *University of Maryland, College Park, MD, United States*
- ⁵⁹ *Syracuse University, Syracuse, NY, United States*
- ⁶⁰ *Pontifícia Universidade Católica do Rio de Janeiro (PUC-Rio), Rio de Janeiro, Brazil, associated to ²*
- ⁶¹ *Institute of Particle Physics, Central China Normal University, Wuhan, Hubei, China, associated to ³*
- ⁶² *Departamento de Física, Universidad Nacional de Colombia, Bogota, Colombia, associated to ⁸*
- ⁶³ *Institut für Physik, Universität Rostock, Rostock, Germany, associated to ¹¹*
- ⁶⁴ *National Research Centre Kurchatov Institute, Moscow, Russia, associated to ³¹*
- ⁶⁵ *Instituto de Física Corpuscular (IFIC), Universitat de Valencia-CSIC, Valencia, Spain, associated to ³⁶*
- ⁶⁶ *Van Swinderen Institute, University of Groningen, Groningen, The Netherlands, associated to ⁴¹*
- ⁶⁷ *Celal Bayar University, Manisa, Turkey, associated to ³⁸*

^a *Universidade Federal do Triângulo Mineiro (UFMT), Uberaba-MG, Brazil*

^b *P.N. Lebedev Physical Institute, Russian Academy of Science (LPI RAS), Moscow, Russia*

^c *Università di Bari, Bari, Italy*

- ^d *Università di Bologna, Bologna, Italy*
- ^e *Università di Cagliari, Cagliari, Italy*
- ^f *Università di Ferrara, Ferrara, Italy*
- ^g *Università di Firenze, Firenze, Italy*
- ^h *Università di Urbino, Urbino, Italy*
- ⁱ *Università di Modena e Reggio Emilia, Modena, Italy*
- ^j *Università di Genova, Genova, Italy*
- ^k *Università di Milano Bicocca, Milano, Italy*
- ^l *Università di Roma Tor Vergata, Roma, Italy*
- ^m *Università di Roma La Sapienza, Roma, Italy*
- ⁿ *Università della Basilicata, Potenza, Italy*
- ^o *AGH - University of Science and Technology, Faculty of Computer Science, Electronics and Telecommunications, Kraków, Poland*
- ^p *LIFAELS, La Salle, Universitat Ramon Llull, Barcelona, Spain*
- ^q *Hanoi University of Science, Hanoi, Viet Nam*
- ^r *Università di Padova, Padova, Italy*
- ^s *Università di Pisa, Pisa, Italy*
- ^t *Scuola Normale Superiore, Pisa, Italy*
- ^u *Università degli Studi di Milano, Milano, Italy*
- ^v *Politecnico di Milano, Milano, Italy*